

# On the Dominance of Trivial Knots among SAPs on a Cubic Lattice

<sup>†</sup>Akihisa Yao, <sup>†</sup>Hiroshi Matsuda, <sup>††</sup>Hiroshi Tsukahara,  
<sup>‡</sup>Miyuki K. Shimamura and <sup>‡</sup>Tetsuo Deguchi

<sup>†</sup>Department of Physics, Faculty of Science and Engineering,  
Chuo University  
1-13-27 Kasuga, Bunkyo-ku, Tokyo 112-8551, Japan

<sup>††</sup>Geographic Information Systems Department,  
Hitachi Software Engineering Co., Ltd.  
Kita-3, Nishi-3, Chuo-ku, Sapporo 060-0003, Japan

<sup>‡</sup>Department of Physics, Faculty of Science  
and Graduate School of Humanities and Sciences,  
Ochanomizu University  
2-1-1 Ohtsuka, Bunkyo-ku, Tokyo 112-8610, Japan

May 20, 2019

## Abstract

The knotting probability is defined by the probability with which an  $N$ -step self-avoiding polygon (SAP) with a fixed type of knot appears in the configuration space. We evaluate these probabilities for some knot types on a simple cubic lattice. For the trivial knot, we find that the knotting probability decays much slower for the SAP on the cubic lattice than for continuum models of the SAP as a function of  $N$ . In particular the characteristic length of the trivial knot that corresponds to a ‘half-life’ of the knotting probability is estimated to be  $2.5 \times 10^5$  on the cubic lattice.

# 1 Introduction

The Self-Avoiding Polygon (SAP) with fixed topology gives a simplified model of real ring polymers in solution that have a topological constraint as well as excluded volume. Throughout the time evolution, a circular polymer keeps the same knot which is given to it when it is made; it does not change its topology under any thermal fluctuations since no crossing through itself is allowed. On the other hand, SAP corresponds to the special case of the Self-Avoiding Walk (SAW) that returns to the origin. If we construct a set of SAPs, then their topological states may contain several different knots. Therefore, it is not trivial how to realize the topological constraint on an SAP. One possible method for assigning the topological constraint on an SAP is that after generating a large number of SAPs we select only such SAPs that have the same given knot. By this method, we can assign the topological constraint on any model of SAP. In this context, the probability that a given SAP has a fixed knot plays a central role, and we call it the *knotting probability* of the model of SAP for the knot. Among many different models, the SAP on the cubic lattice with fixed topology is one of the most fundamental models of SAP. It has an advantage that the definition is very simple. We expect that the model should be suitable for general and mathematical study. In fact, several rigorous results on knotting probability have been derived for the SAP on the cubic lattice [1, 2, 3, 4]. Thus, the main motivation of the present research is to characterize the knotting probability of the SAP on the cubic lattice through numerical simulations.

Let us discuss some previous numerical results on knotting probabilities of SAP [5, 6, 7, 8, 9, 10, 11, 12, 13, 14, 15, 16]. For a model of SAP (or random polygon) with  $N$  steps, we denote by  $P_K(N)$  the knotting probability of the model for knot  $K$ . For the Gaussian model of random polygon and the rod-bead model of SAP, knotting probabilities were evaluated through numerical simulations for the trivial knot  $K = \emptyset$  [6, 8, 10] and also for some non-trivial knots [5, 12, 13, 14, 15]. It was found that for the models of SAP and random polygon, the knotting

probability as a function of the step number  $N$  is given by the following:

$$P_K(N) = C(K)N^{m(K)} \exp[-N/N(K)], \quad (1.1)$$

where  $C(K)$ ,  $m(K)$  and  $N(K)$  are fitting parameters. From the numerical result it was conjectured that the parameter  $N(K)$ , which we call the characteristic length of knot  $K$ , should be given by the same value for any knot  $K$  [12]. Furthermore, it was also conjectured that the parameter  $m(K)$ , which we call the exponent of knot  $K$ , should be universal for different models of SAP or random polygon [13, 14, 15]. We note that the fitting formula (1.1) together with the two conjectures are consistent with the standard asymptotic behavior expected for SAP or random polygon. Here we also note that the rod-bead model is an off-lattice model of SAP.

Recently, the SAP on the cubic lattice with fixed knot was studied through a numerical simulation using the BFACF algorithm, which generates SAPs with the same fixed knot but different step numbers  $N$  [16]. In the simulation, the exponent  $m(K)$  and the growth constant for the number of allowed configurations of the SAP with knot  $K$  has been estimated for some knots. Furthermore, it was shown that the knotting probability for the trivial knot decays “exponentially” for a face-centered cubic lattice [11] and for the cubic lattice [3]. However, any precise estimate of the knotting probability or the characteristic length  $N(K)$  has not been given for the cubic lattice. Thus, it is the primary purpose of this paper to evaluate the characteristic length  $N(K)$  for the SAP on the cubic lattice.

In 1962, Delbrück [17] noticed that the topological constraint may be very important for polymers in biology and chemistry. Since then, the topological problem has been studied in several approaches in physics and mathematics. As one of the earliest studies, des Cloizeaux and Mehta [18] estimated through numerical simulations the critical exponent  $\nu$  for the internal distance of the Gaussian random polygon and discussed some possible properties of random polygons under the topological constraint.

After the rediscovery of the pivot algorithm, many properties of SAW and SAP have been investigated not only in the field theory but also by computer simulations [19, 20]. It seems,

however, that there are only a few works such as [16] where the gyration radius  $\langle R_G^2 \rangle$  of the SAP on the cubic lattice is studied by numerical simulations. Let us denote by  $\langle R_G^2 \rangle_{linear}$  and  $\langle R_G^2 \rangle_{ring}$  the mean square of the gyration radius of SAW and SAP, respectively. It is interesting to evaluate the universal amplitude ratio between  $\langle R_G^2 \rangle_{ring}$  and  $\langle R_G^2 \rangle_{linear}$ . The ratio has been evaluated only up to  $O(\varepsilon)$  in the  $\varepsilon$ -expansion method [21]. Furthermore, according to the scaling theory of polymers, the exponent  $\nu$  for  $\langle R_G^2 \rangle_{ring}$  should be given by that of  $\langle R_G^2 \rangle_{linear}$ . The agreement is confirmed up to  $O(\varepsilon)$  by the renormalization group theory [21, 22]. However, it is nontrivial to confirm the agreement for the SAP on the cubic lattice through numerical simulations. Thus, the numerical study of the gyration radius for the SAP on the cubic lattice is another purpose of this research.

Hereafter in this introduction, we explain some of the main results of our numerical simulations. Employing the pivot algorithm, we construct a large number of SAPs for the SAP on the cubic lattice with given step number  $N$ . For the gyration radius, we have obtained the exponent:  $\nu = 0.5867 \pm 0.0017$ . This is indeed in good agreement with the estimate of the critical exponent of the SAW in the  $\varepsilon$ -expansion:  $\nu = 0.5882 \pm 0.0011$ . Thus, our simulation in the paper also confirms the agreement of the two exponents.

Let us explicitly consider the method for the topological constraint on the SAP in the cubic lattice with given step number  $N$ . The pivot algorithm of the SAP can generate all the allowed configurations of the SAP with equal probability. Therefore, the set of SAPs generated by the algorithm may contain various knots. Suppose that we have constructed  $M$  SAPs of step number  $N$ . Calculating some knot invariants for each of the SAPs, we effectively detect the knot types of the SAPs. We enumerate the number of such SAPs that have the same set of values of the knot invariants for knot  $K$ , and denote it by  $M(K)$ . The expectation value of a physical quantity under the topological constraint with fixed knot  $K$  can be effectively calculated by taking the statistical average of the quantity for the  $M(K)$  SAPs.

We now turn to the knotting probability. Let the symbol  $P_K(N)$  denote the knotting

probability of the SAP with  $N$  steps on the cubic lattice for knot  $K$ . If there are  $M(K)$  SAPs in the total  $M$  SAPs, then we evaluate it by  $P_K(N) = M(K)/M$ . In our simulation,  $10^5$  SAPs ( $M = 10^5$ ) are constructed for six different values of the step number from  $N = 500$  to  $N = 3000$ . We have found that almost all SAPs are topologically equivalent to the trivial knot, and also that the resulting values of the knotting probability for the trivial knot are fitted well by the formula (1.1). Thus, for the trivial knot, we have obtained an estimate of the characteristic length

$$N(\emptyset) = (2.5 \pm 0.3) \times 10^5. \quad (1.2)$$

This result means that trivial knots are dominant among SAPs on the cubic lattice when the step number  $N$  is less than  $10^5$ . It implies that when  $N > N(\emptyset)$ , the majority of SAPs on the cubic lattice have some non-trivial knots. The large value of the characteristic length might be a consequence of strong self-avoiding effect of the SAP on the cubic lattice.

This paper is organized as follows. In section 2 we will explain the pivot algorithm that generates a sequence of SAPs efficiently, and estimate the universal amplitude ratio and the critical exponent  $\nu$  of the gyration radius. We also evaluate the correlation among the generated polygons in the sequence. In section 3 we will explicitly discuss the knotting probability for the trivial knot, and obtain the estimate of the characteristic length. We will also show that the knotting probability for the trivial knot decays almost linearly since the characteristic length of the trivial knot is so large. Finally, we will discuss a possibility that the characteristic lengths take an unique value without depending on knot types, in the last section.

## 2 The mean-square of the gyration radius

### 2.1 Theoretical predictions for SAW and SAP

An  $N$ -step Self-Avoiding Walk (SAW)  $w$  in  $\mathbb{Z}^3$  is a sequence  $w_0, w_1, \dots, w_N$  of  $N+1$  distinct points in  $\mathbb{Z}^3$  such that each point  $w_i$  is one of the nearest neighbors of its predecessor  $w_{i-1}$ :

$|w_i - w_{i-1}| = 1$  for  $i = 1, \dots, N$ . It is also subject to a constraint that any site never be occupied by two or more points in a sequence  $\{w_i\}$ . The points  $w_0$  and  $w_N$  are the endpoints of  $w$ . The components of  $w_i$  are represented by  $w_i^{(\alpha)}$  for  $\alpha = 1, 2, 3$ . The Self-Avoiding Polygon (SAP) is a special case of the SAW that makes a ring. We consider an  $(N - 1)$ -step SAW and denote it by  $w = \{w_0, w_1, \dots, w_{N-1}\}$ . If the endpoint  $w_0$  is the nearest neighbor of the endpoint  $w_{N-1}$ , this is an  $N$ -step SAP in  $\mathbb{Z}^3$ .

The mean-square of the gyration radius of the SAP  $\langle R_G^2 \rangle_{ring}$  is smaller than that of the SAW  $\langle R_G^2 \rangle_{linear}$ . This fact comes from the following difference. The endpoints of SAW are free, while those of SAP are constrained, that is, the endpoints of SAP should meet at the nearest neighbor sites of the lattice. This means that the SAW has a possibility of a longest end-to-end distance whereas the SAP does not.

The RG argument gives several results of the SAW and the SAP. Among these, we are most interested in the amplitude ratio  $\langle R_G^2 \rangle_{ring} / \langle R_G^2 \rangle_{linear}$ . This ratio has been evaluated by using the RG equation and the cluster expansion up to  $O(\varepsilon)$  [21, 22]:

$$\frac{\langle R_G^2 \rangle_{ring}}{\langle R_G^2 \rangle_{linear}} = 0.568. \quad (2.1)$$

According to the RG theory, the amplitude ratio should be universal, *i.e.* it does not depend on the details of the models for the SAW or the SAP. Another interesting result of the RG argument is that the critical exponent  $\nu$  for the mean-square of the gyration radius is universal.

It is well-known that the exponent  $\nu$  of SAW corresponds to the critical exponent of the  $O(n)$  vector model in the limit of  $n$  going to zero. The precise estimate of the critical exponent  $\nu$  of SAW has been made by the  $\varepsilon$ -expansion method through this correspondence [23, 24, 25, 26]:

$$\nu = 0.5882 \pm 0.0011. \quad (2.2)$$

We estimate numerically the mean-square of the gyration radius of the SAP and its critical exponent  $\nu$  in our simulation. We will see that the results of our simulation and the predictions by the RG theory are consistent with each other.

## 2.2 The method of generating SAPs on the cubic lattice

We explain our procedure for generating SAPs on the cubic lattice. We adopt a length-conserving dynamical algorithm, and use the fixed endpoints pivot algorithm. This algorithm was investigated in detail by Madras, Orlitsky, and Shepp [19, 20] and some rigorous results were derived for this algorithm. We call this algorithm MOS pivot for short. The MOS pivot is a highly efficient Monte Carlo method for generating SAWs with fixed endpoints and fixed length. That is, in the Monte Carlo trials of making samples of SAPs, the ratio of the number of successful trials in obtaining ‘correct’ SAPs to that of unsuccessful ones is much larger for the MOS pivot than for other known algorithms. The MOS pivot has the following keywords: micro canonical ensemble, non-local moves and ergodic Markov chains.

We briefly recapitulate the definition and some properties of the MOS pivot. Note that the MOS pivot can be applied in any dimension, though our description is restricted to the cubic lattice case.

The MOS pivot is composed of three kinds of non-local transformations with respect to two given sites  $k, l$  ( $0 \leq k < l \leq N$ ). We define the MOS pivot transformations as follows.

**Definition 1 (Inversion)** *Given an SAW  $w = \{w_0, \dots, w_N\}$  and sites  $k, l$ , define the inversion  $T_{k,l}^{\text{inv}}(w)$  to be the sequence  $w' = \{w'_0, \dots, w'_N\}$  given by*

$$w'_i = \begin{cases} w_k + w_l - w_{k+l-i} & \text{if } k \leq i \leq l \\ w_i & \text{otherwise.} \end{cases}$$

**Definition 2 (Reflection)** *For any SAW  $w$ ,  $0 \leq k < l \leq N$ ,  $m \in \{-1, +1\}$ , and  $1 \leq \alpha < \beta \leq 3$ , define  $T_{k,l:\alpha,\beta}^{\text{ref},m}(w)$  as follows: If  $w_l^{(\alpha)} - w_k^{(\alpha)} \neq m(w_l^{(\beta)} - w_k^{(\beta)})$  or if  $w_l^{(\gamma)} \neq w_k^{(\gamma)}$  for  $\gamma \neq \alpha, \beta$ , then put  $T_{k,l:\alpha,\beta}^{\text{ref},m}(w) = w$ ; otherwise, put  $T_{k,l:\alpha,\beta}^{\text{ref},m}(w) = \{w'_0, \dots, w'_N\}$ , where*

$$w'_i = \begin{cases} w_k^{(\gamma)} - m(w_{k+l-i}^{(\alpha+\beta-\gamma)} - w_l^{(\alpha+\beta-\gamma)}) & \text{if } k \leq i \leq l \text{ and } \gamma \text{ is } \alpha \text{ or } \beta \\ w_i^{(\gamma)} & \text{otherwise.} \end{cases}$$

**Definition 3 (Interchange transformation)** For any SAW  $w$ ,  $0 \leq k < l \leq N$ ,  $m \in \{-1, +1\}$ , and  $1 \leq \alpha < \beta \leq 3$ , define  $T_{k,l;\alpha,\beta}^{\text{int},m}(w)$  as follows: If  $w_l^{(\alpha)} - w_k^{(\alpha)} \neq m(w_l^{(\beta)} - w_k^{(\beta)})$ , then put  $T_{k,l;\alpha,\beta}^{\text{int},m}(w) = w$ ; otherwise, let  $w' \stackrel{\text{def}}{=} T_{k,l;\alpha,\beta}^{\text{int},m}(w)$  be the  $N$ -step walk whose steps  $s'_i \stackrel{\text{def}}{=} w'_i - w'_{i-1}$  are

$$s'_i^{(\gamma)} = \begin{cases} ms_i^{(\beta)} & \text{if } k < i \leq l \text{ and } \gamma = \alpha \\ ms_i^{(\alpha)} & \text{if } k < i \leq l \text{ and } \gamma = \beta \\ s_i^{(\gamma)} & \text{otherwise.} \end{cases}$$

Note that the reflection and the interchange transformations are parameterized by  $(\alpha, \beta, m)$ .

If an operation of one of the three transformations to a given walk makes another walk with a shape different from the original one, we call it a relevant transformation. The result of a relevant transformation is not necessarily an SAW. We note that not all sets of the parameters correspond to relevant transformations. In order to consider only the relevant transformations, we exclude the sets of the parameters for which the reflection and interchange transformations make no change to a given walk:  $T_{k,l;\alpha,\beta}^{\text{ref},m}(w) = w$ ,  $T_{k,l;\alpha,\beta}^{\text{int},m}(w) = w$ . This is a procedure to make an SAW effectively for a simulation. The MOS pivot uses the relevant transformations and works as follows.

- (1) Begin with any SAW  $w$  with step number  $N$ .
- (2) Choose two sites  $k, l$  at random from  $\{0, 1, \dots, N\}$ , where  $k < l$ .
- (3) If a reflection with a set of the parameters is a relevant transformation with respect to  $k$  and  $l$ , write this set of the parameters  $(\alpha, \beta, m)$  in the memory. This procedure repeats for each set of the parameters — for example  $(\alpha, \beta, m) \in \{(1, 2, 1), (2, 3, -1), \dots\}$ . Similarly, write the set of parameters of the interchange transformations for each set of parameters. Then, make the set of the transformation  $\mathcal{F}$ ; for example  $\mathcal{F} = \{T_{k,l}^{\text{inv}}, T_{k,l;1,2}^{\text{ref},1}, T_{k,l;2,3}^{\text{ref},-1}, \dots, T_{k,l;1,2}^{\text{int},1}, T_{k,l;1,3}^{\text{int},-1}, \dots\}$ .
- (4) Choose a transformation  $F$  from the set  $\mathcal{F}$  and construct a walk  $F(w)$ .
- (5) If  $F(w)$  is an SAW, we accept it as a correct SAW. Otherwise we discard it.



The fact that this algorithm is ergodic is proven by Madras *et al.* [20].

We construct a ‘seed’ SAP by combining two SAWs which have the same endpoints. First we make an  $N/2$ -step SAW using the myopic self-avoiding walk (MSAW) algorithm [27], where  $N$  is an even integer. Secondly we perform the MOS pivot transformation with respect to  $k = 0, l = N/2$ . Finally we concatenate the endpoints of the new and original SAWs respectively (figure 1) and get an SAP with the step number  $N$  if it has no self-intersections.

We make a sequence of SAPs for a simulation. If the MOS pivot transformation changes a given SAP into a different SAP, this operation is called a successful MOS pivot. To simplify the explanation, we introduce an operator  $p$  that is a successful MOS pivot and define  $p^n$  as the operator that operates  $p$  on a given SAP  $n$  times. We construct a seed SAP  $w$  and make  $p$  operate on  $w$ . Then, we get a new SAP  $p(w)$ . To make another SAP, we operate  $p$  on  $p(w)$  again — namely,  $p^2(w) = p(p(w))$ . Thus, we apply to a seed SAP the operator  $p^n$  for each  $n$  and then obtain a sequence of SAPs  $\{w, p(w), p^2(w), p^3(w), \dots\}$ .

For generating SAPs, we use the Mersenne Twister that is a pseudo random number generator [28]. This algorithm has the following properties: (1) we can get many samples because the period is  $2^{19937} - 1$ , (2) we treat high dimensional space (max 623 dimensions), (3) pseudo random numbers are generated fast and (4) we can use the memory efficiently. Thus, the Mersenne Twister is a high performance generator.

## 2.3 The pivot correlations

In this section we show how the random sampling from the configuration space of SAP with fixed-length is simulated by the MOS pivot. It is obvious that the two SAPs, one of which is a seed SAP and the other an SAP generated by a single successful MOS pivot from the seed SAP, are not independent but are correlated, in particular in local shapes of them. Thus, it is necessary to evaluate the decay of the correlation under the operations of the MOS pivot.

We regard the number  $\tau$  of operations of successful MOS pivots as the time of evolution of

the shape of SAP under the MOS pivot operations:  $p^\tau(w) = w(\tau)$  ( $\tau > 0$ ),  $w = w(0)$  ( $\tau = 0$ ) and  $w$  is a seed SAP. Then we define the correlation function for the structure of SAP with the step number  $N$  by

$$C(\tau) = \frac{\sum_{\alpha=1}^3 \sum_{i=0}^{N-1} \left\langle \left( w_i^{(\alpha)}(0) - \frac{1}{N} \sum_{j=0}^{N-1} w_j^{(\alpha)}(0) \right) \left( w_i^{(\alpha)}(\tau) - \frac{1}{N} \sum_{l=0}^{N-1} w_l^{(\alpha)}(\tau) \right) \right\rangle}{\sum_{\alpha=1}^3 \sum_{i=0}^{N-1} \left\langle \left( w_i^{(\alpha)}(0) - \frac{1}{N} \sum_{j=0}^{N-1} w_j^{(\alpha)}(0) \right)^2 \right\rangle}, \quad (2.3)$$

where  $w_i^{(\alpha)}(\tau)$  is the  $\alpha$ -component of the  $i$ -th site of SAP (or SAW) after  $\tau$  pivot operations and  $\langle \cdot \rangle$  denotes the statistical average.

To calculate physical quantities of SAPs, for example the mean-square of the gyration radius, we have to generate samples which are randomly chosen from the configuration space of SAP. After operating the successful MOS pivots several times the correlation decays almost completely, and the SAP, thus obtained, is effectively independent of the original SAP. This is the way of random sampling in the dynamical Monte Carlo method. The distribution over the configuration space of SAP thus obtained is then viewed effectively as uniform. This is expected from the application of the theory of the Markov chain and the fact that the transitional probability of the MOS pivot is symmetric.

In our simulation, we evaluated the correlations of SAPs with the step number  $N$  at 500 and 1,000, and generated 10,000 sequences (starting from 10,000 different seeds) to take the statistical average. In figure 2a and 2b, we plot the correlation  $C(\tau)$  versus the time  $\tau$  in the case of  $N = 500$  and 1,000, respectively. Error bars show one standard deviation which are estimated by assuming that the data follows the Poisson distribution.

Note that the number of independent transformations for the normal pivot algorithm [19, 27] is  $d!2^d - 1$  (the normal pivot algorithm is an algorithm with one endpoint free while the other fixed), which correspond to the number of all the elements of  $d$ -dimensional orthogonal group on a hypercubic lattice, while for the MOS pivot  $2d(d-1) + 1$  in the  $d$ -dimensional hypercubic lattice. In the cubic lattice, the MOS pivot has 13 pivot transformations while the normal pivot algorithm has 47. Because of this large difference in the freedom of pivot transformations, the

decay rate of the correlation function  $C(\tau)$  is slower in the case of the MOS pivot than in the case of normal pivot algorithm (figure 2a and 2b).

Our evaluation of the correlation  $C(\tau)$  for the MOS pivot shows that the correlation decays almost completely when 200 successful MOS pivots are operated, and the original SAP  $w$  and  $p^{200}(w) = w(200)$  can be regarded as independent each other. Thus, we define the operator  $P$  by  $P = p^{200}$  and generate a sequence  $\{w^{[1]}, w^{[2]}, \dots, w^{[t-1]}, w^{[t]}, \dots\}$ , where  $w^{[t]} = P(w^{[t-1]})$  and  $w^{[0]} = w(0)$ . Elements in this sequence are independent of one another and distributed uniformly over the configuration space of SAP with fixed-length.

Generating many such sequences, we evaluate statistical quantities for the SAP, in particular the amplitude ratio  $\langle R_G^2 \rangle_{ring} / \langle R_G^2 \rangle_{linear}$  and the mean-square of the gyration radius. Applying the MOS pivot to the knotting probability, we should consider statistics of knotted polygons generated in our simulation. We will see this in the section 3.2.

## 2.4 The amplitude ratio and the critical exponent $\nu$

We calculate the ratio  $\langle R_G^2 \rangle_{ring} / \langle R_G^2 \rangle_{linear}$  and the exponent  $\nu$  using the MOS pivot and compare resulting values with theoretical and other simulated values. The mean-square of the gyration radius is calculated by

$$\langle R_G^2 \rangle = \frac{1}{T} \sum_{t=1}^T \left[ \frac{1}{N} \sum_{i=0}^N \left( w_i^{[t]} - \frac{1}{N} \sum_{j=0}^N w_j^{[t]} \right)^2 \right], \quad (2.4)$$

where  $w_i^{[t]}$  denotes the  $i$ -th site in  $t$ -th SAP,  $T$  is the number of polygons and  $N$  the step number. It has been proposed that the gyration radius should have the asymptotic behavior

$$\langle R_G^2 \rangle = AN^{2\nu}(1 + BN^{-\Delta}) \quad \text{as } N \rightarrow \infty. \quad (2.5)$$

Choosing  $\frac{1}{2}$  for the exponent  $\Delta$  of the correction term, the numerical data given by the equation (2.4) are plotted in figure 3 and fitted to  $AN^{2\nu}(1 + BN^{-\frac{1}{2}})$ , where  $A$ ,  $B$  and  $\nu$  are fitting parameters. Since there are not enough data to fit in a four-parameter curve in our

simulation, we have assumed the fixed value for the exponent  $\Delta$ . We plot the mean-square of the gyration radius from  $N = 500$  to  $N = 30,000$  in figure 3. Here, we set  $T$ , the number of polygons, to 10,000. The error bars denote one standard deviation given by the Poisson distribution to the number  $T$  of polygons with  $N$ .

The three parameters are obtained by fitting the data in figure 3

$$\nu = 0.5867 \pm 0.0017, \quad (2.6)$$

$$A = 0.1101 \pm 0.0037, \quad (2.7)$$

$$B = -0.06 \pm 0.04. \quad (2.8)$$

The errors are subjective 68.3% confidence intervals. For the SAW, Madras *et al.* [19] estimated the exponent  $\nu$  by the pivot algorithm up to  $N = 80,000$ :

$$\nu = 0.5877 \pm 0.0006, \quad (2.9)$$

$$A = 0.19455 \pm 0.00007, \quad (2.10)$$

$$B' = -0.11432 \pm 0.00465, \quad (2.11)$$

$$\Delta = 0.56 \pm 0.03. \quad (2.12)$$

Here,  $B'$  corresponds to  $AB$  in our estimated values.

From (2.7) and (2.10), we obtain the amplitude ratio

$$\frac{\langle R_G^2 \rangle_{ring}}{\langle R_G^2 \rangle_{linear}} = 0.566 \pm 0.019, \quad (2.13)$$

where an error is a subjective 68.3% confidence interval. Our estimated value of the amplitude ratio is consistent with the value of the RG argument (2.1) up to  $O(\varepsilon)$ . The exponent value (2.6) is also in good agreement with that of the RG argument (2.2) and that of the simulation for the SAW (2.9).

### 3 The characteristic length $N(\emptyset)$

### 3.1 A method of evaluation of the knotting probability

We evaluate the knotting probability in the following way. We generate  $M$  SAPs of  $N$  steps and then enumerate the number  $M(K)$  of those polygons which are equivalent to a given knot type  $K$ . We define the knotting probability  $P_K(N)$  by the ratio  $M(K)/M$ .

In our simulation, we determine knot types of SAPs using the 2nd-order Vassiliev-type invariant and the Alexander polynomial evaluated at  $t = -1$ . The Vassiliev-type invariants have the following advantages: (1) we can calculate them in polynomial time, and (2) we can calculate them without consuming a large memory area [29]. The Vassiliev-type invariants are not complete invariants. However, in the practical sense we can safely say that if the value of the Vassiliev-type invariant computed for an SAP is zero, this SAP is a trivial knot. We will see in section 3.3 that complicated knots are very rare events in our data. Even if non-trivial knots are misidentified as the trivial knot by the Vassiliev-type invariant (this chance is very small), it would not affect the results of this paper.

For calculating the knotting probability, we generate random sequences of SAPs. We make five seeds for each of the six step numbers  $N = 500, 1,000, 1,500, 2,000, 2,500$ , and  $3,000$ , and operate  $P$  on them. Recall that the operator  $P = p^{200}$  is defined by 200 successful MOS pivots. Then, we get effectively random sequences of SAPs. A sequence of SAPs derived from each seed has a set of 20,000 SAPs. For each step number  $N$ , we thus get samples of 100,000 SAPs.

In order to analyze the behavior of the knotting probability, we use the fitting formula (1.1). Here, we write it again:

$$P_K(N) = C(K)N^{m(K)} \exp \left[ -\frac{N}{N(K)} \right],$$

where  $C(N)$ ,  $N(K)$ , and  $m(K)$  are fitting parameters. In particular  $N(K)$  is called characteristic length with knot type  $K$ . This formula was introduced by Deguchi and Tsurusaki [12, 14, 15]. They pointed out that the formula (1.1) is suitable for the knotting probabilities of the Gaussian and rod-bead models. We will show that this is suitable also for the knotting probability  $P_K(N)$

of the cubic lattice model.

### 3.2 The random events of knotted polygons

Let us discuss statistics of knotted polygons generated in our simulation. We will see in section 3.3 that almost all polygons are of trivial knots. Therefore, we may assume that non-trivial knots are generated such as the Poisson random events: the number of trivial knots between two knotted SAPs will follow the Poisson distribution, if the SAPs are randomly constructed.

Let us consider the “time interval” of the Poisson random events. We recall that the time is a discrete number. We measure the length  $L$  of the time interval of SAPs from time  $t_1$  at which a knotted SAP appears to time  $t_2$  at which the next knotted SAP appears after  $t_1$ , and set  $L = t_2 - t_1$ . If non-trivial knots are generated as the Poisson random events, the time interval  $L$  follows the function:

$$D(N, L) = A(N) P_{\emptyset}(N)^{L-1}. \quad (3.1)$$

We call it the discrete distribution function of the time interval  $L$ . Here,  $P_{\emptyset}(N)$  is the knotting probability for the trivial knot. We have introduced  $A(N)$  for a technical reason and hence  $D(N, L)$  is not necessarily normalized.

The discrete distribution functions of the time interval  $L$  are numerically evaluated as follows. The time interval  $L$  is a discrete random variable. We introduce a sequence of natural numbers  $\{l_0, l_1, \dots\}$ , where  $l_i = 50 \times i$ . Then, we count the number of polygons with  $L$  taking values in  $[l_i, l_{i+1})$  and plot it at  $l_i$  for each  $i$ . This is the discrete distribution function of the time interval  $L$  obtained from numerical evaluation.

We plot the discrete distribution functions obtained by the numerical evaluation and  $D(N, L)$  as a function of  $L$ , where  $P_{\emptyset}(N)$  is estimated from table 1 and  $A(N)$  is chosen to fit these distributions (See figure 4a and 4b). Error bars denote one standard deviation. They are estimated by applying the Poisson distribution to the number of samples included in interval  $L$ . For  $N = 1,000, 1,500, 2,000, 2,500$ , and  $3,000$ , these graphs show a fairly good agreement

with the function  $D(N, L)$ . In the case of  $N = 500$ , the data deviate from the function. This is not unexpected since we have too few samples of knotted polygons. We do not plot the graph for  $N = 500$  in this paper.

We expect from figure 4a and 4b that the MOS pivot makes a uniform ensemble for knots. Thus, we can calculate the knotting probability and the characteristic length using the MOS pivot.

### 3.3 The number of unknotted polygons

The table 1 gives the number of each knot type with respect to  $N$ . Here, errors correspond to 68.3% confidence intervals. They are estimated by applying the binomial distribution to the number  $M(K)$  of polygons for knot  $K$ . In the table 1 we explain the notations:  $\emptyset, 3_1, 4_1$  denote the trivial knot, the trefoil knot and the figure eight knot, respectively. The other knot types are denoted by *etc.*

The table 1 tells clearly that almost all the generated SAPs are trivial knots.  $M(3_1)$  is also much larger than  $M(4_1)$ . The other knots (*etc.*) are nearly equal to zero.

Step Numbers	$M(\emptyset)$	$M(3_1)$	$M(4_1)$	<b>etc.</b>	$M$
500	$99,849 \pm 25$	$147 \pm 24$	$3 \pm 3$	$1 \pm 1$	100,000
1,000	$99,640 \pm 38$	$344 \pm 37$	$9 \pm 6$	$7 \pm 5$	100,000
1,500	$99,430 \pm 48$	$541 \pm 46$	$24 \pm 10$	$5 \pm 4$	100,000
2,000	$99,208 \pm 56$	$752 \pm 55$	$27 \pm 10$	$13 \pm 7$	100,000
2,500	$98,965 \pm 64$	$985 \pm 62$	$38 \pm 12$	$12 \pm 7$	100,000
3,000	$98,787 \pm 69$	$1,157 \pm 68$	$40 \pm 13$	$16 \pm 8$	100,000

Table 1: the Number of Generated Knots  
The estimated errors correspond to one standard deviation.

Next we focus on the knotting probability for the trivial knot, and plot  $P_\emptyset(N)$  as a function of  $N$  (figure 5). The error bars are one standard deviation.  $P_\emptyset(N)$  decays linearly with respect to  $N$ . It is expected that  $P_\emptyset(N)$  becomes exponential decay when  $N$  goes to infinity. In [1, 2, 3]

it was shown that the knotting probability  $P_\emptyset(N)$  tends to zero “exponentially”:

$$P_\emptyset(N) = A \exp[-\kappa N + o(N)], \quad \text{when } N \rightarrow \infty. \quad (3.2)$$

Thus, this is a natural situation.

The asymptotic shape (3.2) is realized for the trivial knot in our case when the fitting parameters of the formula (1.1) take the following values:  $|m(\emptyset)| \ll 1$  and  $C(\emptyset) \simeq 1$ . In fact, using the least-squares estimation, we find:

$$C(\emptyset) = 1.0035 \pm 0.0035 \quad (3.3)$$

$$m(\emptyset) = (-4.7 \pm 5.7) \times 10^{-4} \quad (3.4)$$

$$N(\emptyset) = (2.5 \pm 0.3) \times 10^5 \quad (3.5)$$

$$\chi^2 = 0.748 \quad (3.6)$$

$$Prob(\chi^2 > 0.748) = 0.862 \quad (3.7)$$

(errors are one standard deviation). Here, the  $\chi^2$  value (*i.e.* sum of square of normalized deviations from the regression line) can serve as a criterion of good fit. It should be distributed as  $\chi^2$  with  $n - 3$  degrees of freedom, where  $n$  is the number of data points in the fit.  $Prob(\chi^2 > 0.748)$  is the probability that  $\chi^2$  would exceed the observed value, in this case 86.2%. This implies that the formula (1.1) is suitable. It is remarkable that the characteristic length of the trivial knot is much larger than the value expected from the rod-bead model.

There have been a few simulation studies on several lattices. In [11] the knotting probability for the trivial knot was calculated on a face-centered cubic (FCC) lattice. It was shown that assuming the two-parameter fitting formula:  $P_\emptyset(N) = C(\emptyset)e^{-\alpha(\emptyset)N}$ , the parameters were given



by

$$\begin{aligned}
\alpha(\emptyset) &= (7.6 \pm 0.9) \times 10^{-6} \\
C(\emptyset) &= 1.0011 \pm 0.003 \\
\chi^2 &= 2.7 \\
Prob(\chi^2 > 2.7) &= 0.44,
\end{aligned}$$

where errors were one standard deviation. Our interpretation of  $\alpha(\emptyset)$  taking  $7.6 \times 10^{-6}$  is that the characteristic length is  $1.3 \times 10^5$ . Comparing the cubic lattice with the FCC lattice, the characteristic length is larger on the cubic lattice than on the FCC lattice. In [3] it was also shown that the exponent  $\alpha(\emptyset)$  in the above form was  $(5.7 \pm 0.5) \times 10^{-6}$  on the cubic lattice. This corresponds to the characteristic length of  $1.8 \times 10^5$ . We can expect that this is consistent with our estimated value within the error bars. Now we return to our results of fitting to our data. We estimate not only the characteristic length  $N(\emptyset) \simeq 2.5 \times 10^5$  but also the exponent of a correction term  $m(\emptyset) \simeq 0$ . These parameters show that the knotting probability for the trivial knot serves a “pure exponential” decay on the cubic lattice. This is a new result for the cubic lattice model. Thus, the simulation in the paper improves that of [3].

We have several interpretations of the characteristic length  $N(\emptyset)$ . Since  $N(\emptyset)$  is so large, we found that the number of knotted polygons are much smaller than that of unknotted polygons in our simulation. We expect that the knotting probability for the trivial knot decreases to about 30% at  $N = N(\emptyset)$ . Thus, non-trivial knots become majority of SAPs when  $N$  is larger than  $N(\emptyset)$ . In addition to this, we will see in section 4 that  $N(\emptyset) \simeq N(K)$  for any knot type  $K$  is due to the fact that  $N(\emptyset)$  is large.

In figure 6, we plot the knotting probability for the trefoil knot  $P_{3_1}(N)$  as a function of  $N$ , where error bars are one standard deviation. The data points almost lie on a straight line. Since the data of the trefoil knot are only six points in the step number, we cannot fit the knotting probability  $P_{3_1}(N)$  to formula (1.1). We leave deciding fitting parameters for the trefoil knot

or more complicated knots as future investigations.

The knotting probability  $P_{3_1}(N)$  may have a finite-size effect. When we set  $m(3_1) = 1$  as expected from [16, 14], the formula (1.1) does not match with  $P_{3_1}(N)$  in our data. Deguchi and Tsurusaki argued that a finite-size effect appeared in the knotting probabilities in [14]. When we plot the straight line fitted to  $P_{3_1}(N)$ , the line intersects with the  $x$ -axis at a positive value. This is the finite-size effect. We introduce offset parameter  $N_{ini}$  and replace  $N$  by  $\tilde{N} = N - N_{ini}$  in the formula (1.1). When we fix  $m(3_1) = 1$ , our rough estimation gives as  $N_{ini} \sim 140$  for the trefoil knot. On the other hand, we roughly estimate  $N_{ini} \sim 0$  for the trivial knot. We expect that such finite-size effect would also appear in the knotting probabilities for the SAPs with more complicated knot types. It could be confirmed by generating SAPs with much larger  $N$ .

In section 2.4 we calculated the gyration radius including all possible knots, and then estimated the universal amplitude ratio and the universal exponent  $\nu$ . Without classifying knot types, however, we can effectively consider only trivial knots when  $N < N(\emptyset)$ . The universal amplitude ratio and the universal exponent are evaluated effectively for the trivial knots, although 2% of the SAPs are non-trivial knots and we neglect their influence.

## 4 A consequence of the large characteristic length $N(\emptyset)$

The trivial knot dominates among SAPs on the cubic lattice when  $N$  is less than  $2.5 \times 10^5$ . Our interpretation is that the cubic lattice has so strongly the excluded-volume effect that it almost prevents appearances of knotted polygons.

We have a conjecture that the appearance of a complicated knot is a rare event on the cubic lattice. According to [12, 14, 15], non-trivial knots occupy a large number of configurations of SAPs for  $N \geq N(\emptyset)$ . We believe that the above situation is realized also on the cubic lattice. If the formula (1.1) is a suitable form of the knotting probability and if the trefoil and figure eight knots on the cubic lattice behave like these of continuum models, the ratio  $M(4_1)/M(3_1)$  for each

step number  $N$  should depend only on the ratio  $C(4_1)/C(3_1)$ . We recall that  $M(3_1) \gg M(4_1)$  for  $N < 3,000$  from the table 1. Then, at  $N \sim 2.5 \times 10^5$  almost all SAPs are expected to be  $3_1$  knotted polygons on the cubic lattice unlike SAPs on continuum models.

We see that our estimated value  $N(\emptyset)$  is related to the growth constant  $\mu$  from the viewpoint of Orlandini *et al.*[16]. The asymptotic behavior of the number of  $N$ -step polygons  $c_N$  is given by

$$c_N = aN^{\alpha-3}\mu^N \left(1 + bN^{-\Delta} + o(N^{-1})\right), \quad (4.1)$$

where  $\alpha$  and  $\Delta$  are critical exponents. For fixed knot type  $K$ , it is believed that the number  $c_N(K)$  of polygons with knot  $K$  should have a similar form:

$$c_N(K) = a(K)N^{\alpha(K)-3}\mu(K)^N \left(1 + b(K)N^{-\Delta(K)} + o(N^{-1})\right). \quad (4.2)$$

Then, the knotting probability  $P_K(N)$  is given by  $c_N(K)/c_N$ , and this implies that the characteristic length  $N(\emptyset)$  relates to the growth constants  $\mu$  and  $\mu(\emptyset)$ . We can estimate the ratio  $\mu/\mu(\emptyset)$  from the value of  $N(\emptyset)$ :

$$\frac{\mu}{\mu(\emptyset)} \simeq e^{1/N(\emptyset)} \sim 1 + (4 \pm 2) \times 10^{-6}, \quad (4.3)$$

where an error is two standard deviations.

Let us discuss the independence of the characteristic length  $N(K)$  with respect to knot type  $K$ . Orlandini *et al.* [16] calculated the growth constants directly and showed the following equality:

$$\mu(\emptyset) = \mu(K) = 4.6836 \pm 0.0038 \quad \text{for any knot type } K, \quad (4.4)$$

where an error corresponds to 95% confidence interval. In addition Guttmann estimated the growth constant [30]

$$\mu = 4.68393 \pm 0.00002 \quad (4.5)$$

using exact enumeration and series analysis (an error is one standard deviation). From (4.4) and (4.5), we obtain the ratio

$$\frac{\mu}{\mu(\emptyset)} = \frac{\mu}{\mu(K)} \simeq 1 + (7 \pm 8) \times 10^{-5}, \quad (4.6)$$

where an error is two standard deviations. From (4.3) and (4.6), we expect that the characteristic length is independent of the knot type:  $N(\emptyset) \simeq N(K) \sim 2.5 \times 10^5$  for any knot type  $K$ .

Although the independence of  $\mu(K)$  with respect to knot type  $K$  is pointed out by Orlandini *et al.* [16], we can also confirm it more precisely through our simulation. While Orlandini *et al.* [16] calculated the growth constants, we have no direct calculation of them. However, we can predict that the difference between  $\mu(\emptyset)$  and  $\mu(K)$  is very small when we use the following inequalities:  $\liminf_{N \rightarrow \infty} N^{-1} \log c_N(K) \geq \mu(\emptyset)$  and  $\limsup_{N \rightarrow \infty} N^{-1} \log c_N(K) < \mu$  for any knot type  $K$ , which were proven in [4, 3]. If both  $\liminf_{N \rightarrow \infty} N^{-1} \log c_N(K)$  and  $\limsup_{N \rightarrow \infty} N^{-1} \log c_N(K)$  exist and take the same value  $\mu(K)$ , then we have  $\mu(\emptyset) \leq \mu(K) < \mu$ . These inequalities and the estimate (4.3) limit the ratio  $\mu(K)/\mu(\emptyset)$  to

$$\left| \frac{\mu(K)}{\mu(\emptyset)} - 1 \right| \leq (4 \pm 2) \times 10^{-6}. \quad (4.7)$$

This is a strong bound. Thus, we can expect that  $\mu(\emptyset) \simeq \mu(K)$  for any knot type  $K$ .

## Acknowledgement

We would like to thank Takeo Inami for a careful reading of the manuscript and valuable comments. A.Y. is supported by a Research Assistant Fellowship of Chuo University. This work is supported partially by the Grant-in-Aid for Encouragement of Young Scientists (No. 12740231).

## References

- [1] D.W. Sumners and S.G. Whittington, *J. Phys. A.* **21**,1689 (1988).

- [2] N. Pippenger, *Discrete Appl. Lett. Math.* **25**,273 (1989).
- [3] S.G. Whittington, *AMS Proc. Symp. Applied Math.* **45**,73 (1992).
- [4] C.E. Soteros, D.W. Sumners, and S.G. Whittington, *Math. Proc. Camb. Phil. Soc.* **111**,75 (1992).
- [5] A.V. Vologodskii, A.V. Lukashin, M.D. Frank-Kamenetskii, and V.V. Anshelevich, *Sov. Phys. JETP* **39**,1059 (1974).
- [6] J.P.J. Michels and F.W. Wiegel, *Phys. Lett. A* **90**,381 (1982).
- [7] M. Le Bret, *Biopolymers* **19**,619 (1980).
- [8] Y.D. Chen, *J. Chem. Phys.* **74**,2034 (1981); *J. Chem. Phys.* **75**,2447 (1981); *J. Chem. Phys.* **75**,5160 (1981).
- [9] K.V. Klenin, A.V. Vologodskii, V.V. Anshelevich, A.M. Dykhne and M.D. Frank-Kamenetskii, *J. Biomol. Struct. Dyn.* **5**,1173 (1988).
- [10] K. Koniaris and M. Muthukumar, *Phys. Rev. Lett.* **66**,2211 (1991).
- [11] E.J.J. van Rensburg and S.G. Whittington, *J. Phys. A* **23**,3573 (1990).
- [12] T. Deguchi and K. Tsurusaki, *J. Knot Theory and Its Ramifications* **3**,321 (1994).
- [13] T. Deguchi and K. Tsurusaki, in *Geometry and Physics*, Lect. Notes in Pure and Applied Math. Series/184, ed. by J.E. Andersen, J. Dupont, H. Pedersen, and A. Swann, (Marcel Dekker Inc., Basel Switzerland, 1997), pp. 557-565. (the Proceedings of *Geometry and Physics*, Institute of Mathematics, University of Aarhus, 18th-27th July, 1995, Aarhus, Denmark.)
- [14] T. Deguchi and K. Tsurusaki, *Phys. Rev.E* **55**,6245 (1997).
- [15] T. Deguchi and K. Tsurusaki, *Lectures at Knots96*, 95 (World Scientific, 1997).
- [16] E. Orlandini, M.C. Tesi, E.J.J. van Rensburg, and S.G. Whittington, *J. Phys. A* **31**,5953 (1998).

- [17] M. Delbrück, *Proc. Symp. Appl. Math* **4**,55 (1962).
- [18] J. des Cloizeaux and M.L. Mehta, *J. Phys. (Paris)* **40**,665 (1979).
- [19] B. Li, N. Madras and A.D. Sokal, *J. Stat. Phys.*, **80**,661 (1995).
- [20] N. Madras, A. Orlicsky, and L.A. Shepp, *J. Stat. Phys.*, **58**,159 (1990).
- [21] J.J. Prentis, *J. Chem. Phys.* **76**,1574 (1982).
- [22] M. Lipkin, Y. Oono, and K.F. Freed *Macromolecules* **14**,1270 (1981).
- [23] J.C. LeGuillou and J. Zinn-Justin, *Phys. Rev. B.*, **21**,3976 (1980).
- [24] J.C. LeGuillou and J. Zinn-Justin, *J. Phys. Lett.*, **46**,L-137 (1985).
- [25] J.C. LeGuillou and J. Zinn-Justin, *J. Phys. (Paris)*, **50**,1365 (1989).
- [26] R. Guida and J. Zinn-Justin, *Preprint SPhT-t97/040*.
- [27] N. Madras G. Slade, *“The Self-Avoiding Walk”* (Birkhäuser, 1993).
- [28] <http://www.math.keio.ac.jp/matsumoto/emt.html>
- [29] T. Deguchi and K. Tsurusaki, *Phys. Lett. A* **174**,29 (1993).
- [30] A.J. Guttmann, *J. Phys. A* **22**,2807 (1989).

## Figure Caption

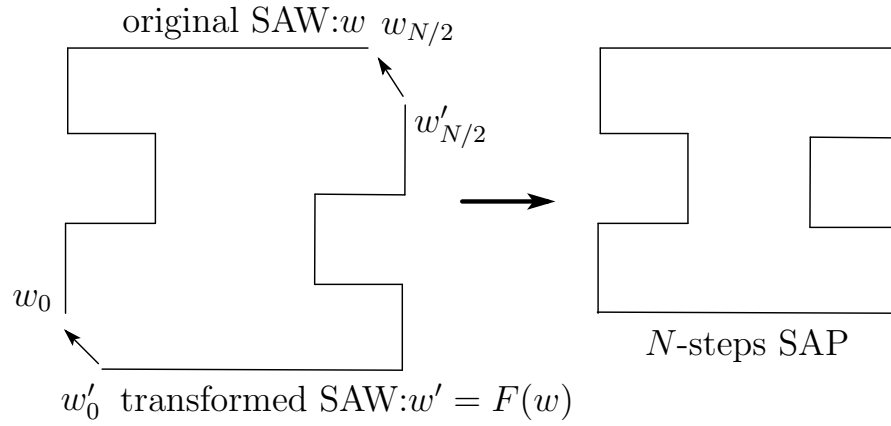


Figure 1: Generated Seed SAP with Step Number  $N$

An original SAW  $w$  generated by the MSAW algorithm with the step number  $N/2$  transforms into another SAW using the MOS pivot with respect to  $k = 0$  and  $l = N/2$ . We concatenate the edges of new and original SAWs, respectively. We get an  $N$ -step SAP.

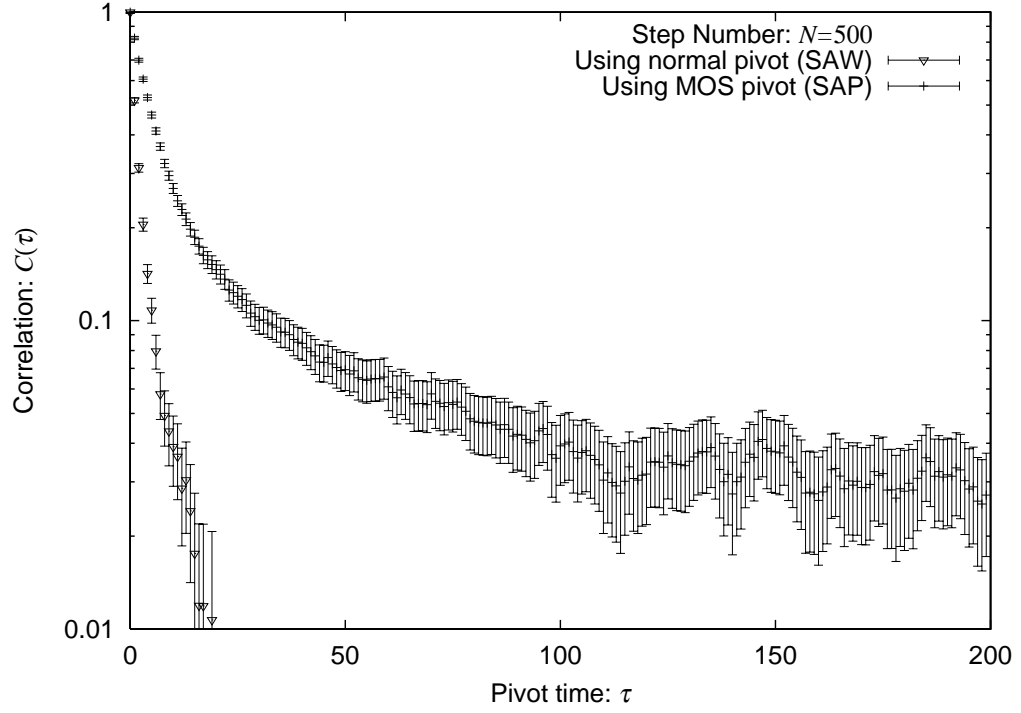


Figure 2a: Pivot Correlation  $C(\tau)$  at  $N = 500$

We plot the pivot correlations  $C(\tau)$  versus the time  $\tau$ . The MOS pivot and the normal pivot operations in the case of  $N = 500$ , respectively. Here, the  $\tau$  is the number of trials, and error bars correspond to one standard deviation. The correlation of the MOS pivot decays slower than that of the normal pivot.



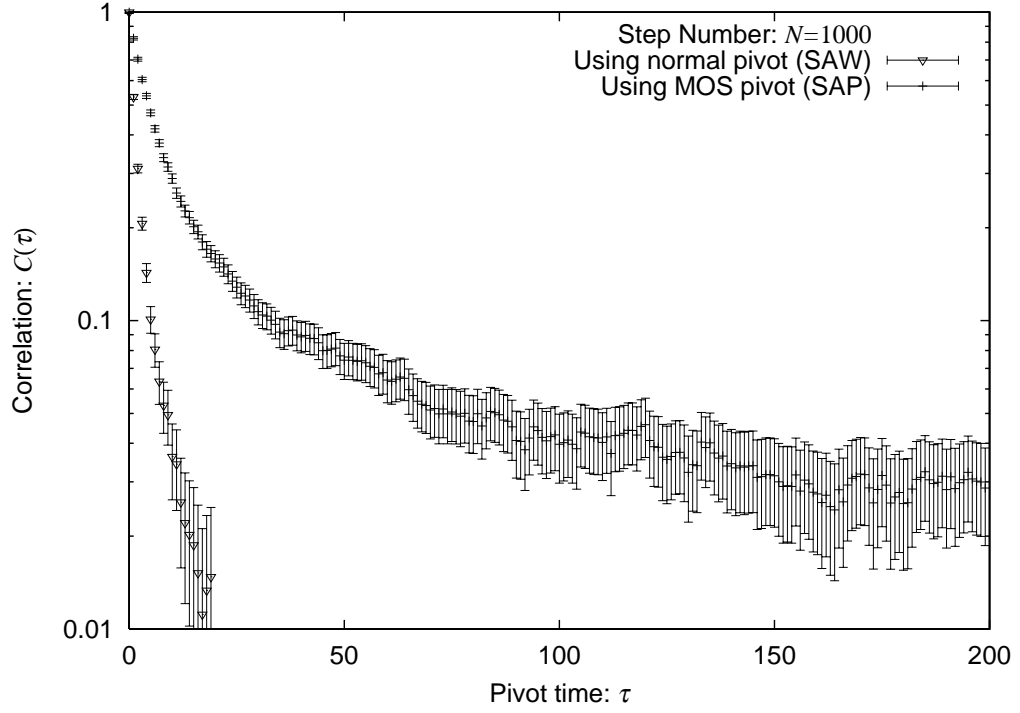


Figure 2b: Pivot Correlation  $C(\tau)$  at  $N = 1000$

Similarly to the Fig.2a we plot the pivot correlations  $C(\tau)$  versus the time  $\tau$ . The MOS pivot and the normal pivot operations in the case of  $N = 1000$ , respectively. Here, the  $\tau$  is the number of trials, and error bars correspond to one standard deviation. At  $\tau = 200$ , we consider correlations  $C(\tau)$  as zero focusing on the MOS pivot correlations for  $N = 500$  and  $1000$ .

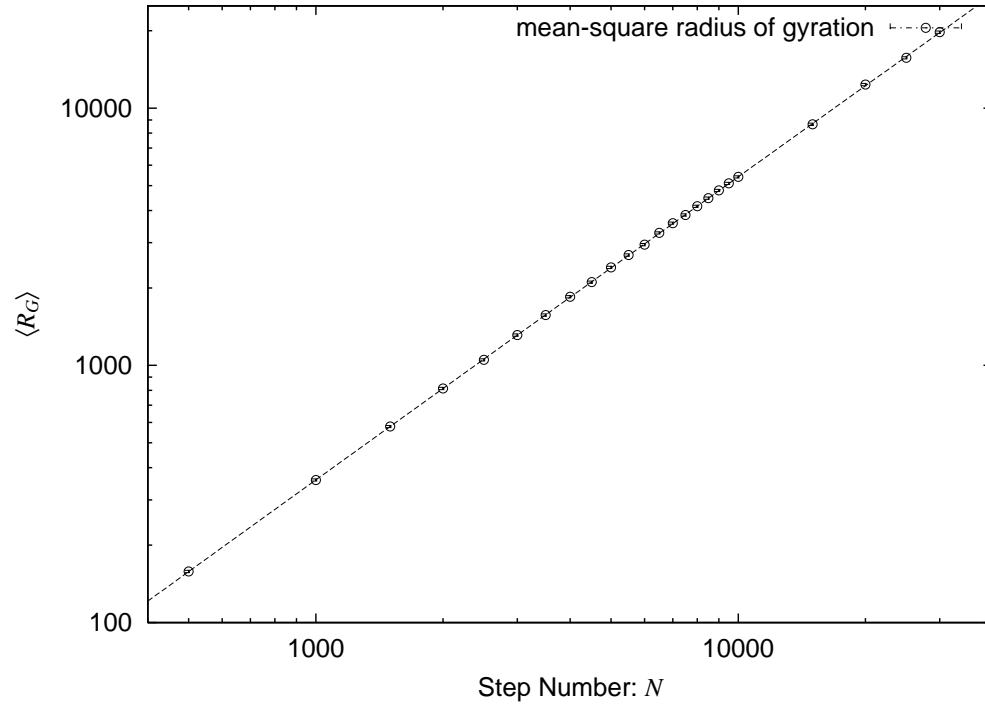


Figure 3: Mean-Square Radius of Gyration  $\langle R_G \rangle$

We give the log-log plotted graph of the mean-square of gyration radius versus the step number  $N$ . Here error bars denote one standard deviation.

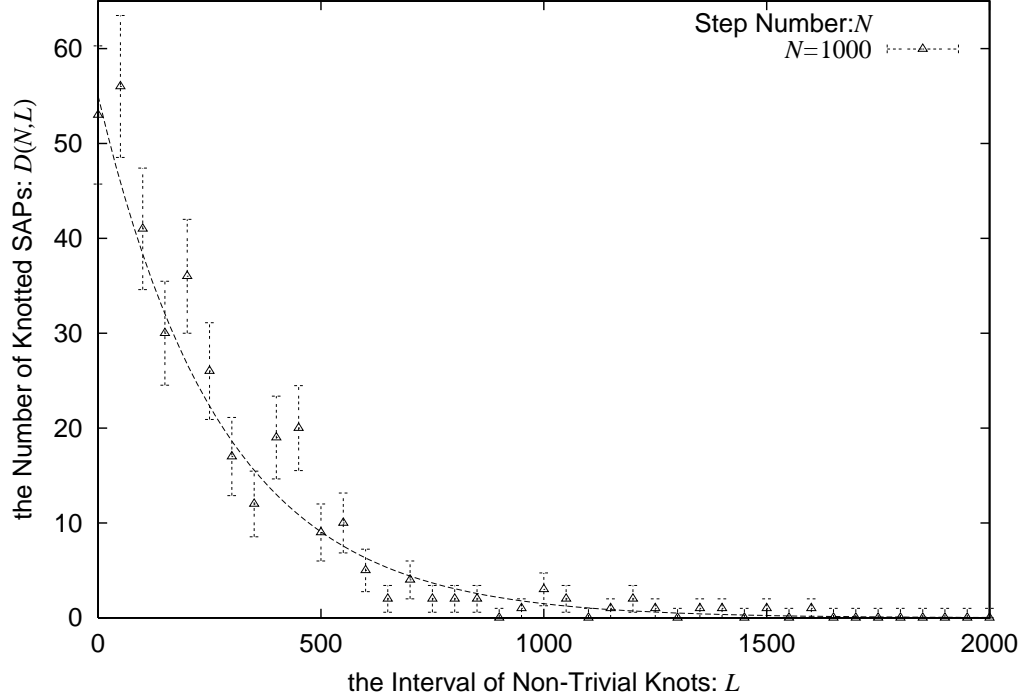


Figure 4a: Discrete Distribution Function of Interval  $L$  of Non-Trivial Knots for  $N = 1000$

The number of occurring a knotted SAP with respect to the time interval  $L$  is represented by the Poisson distribution:  $D(N, L) = A(N)P_0(N)^L$ .  $P_0(N)$  is the knotting probability of the trivial knot with the step number  $N$  and  $A(N)$  is a normalization factor. We call it the discrete distribution function of the time interval  $L$ . In our simulation, we count the number of polygons with  $L$  taking values in  $[l_i, l_{i+1})$  and plot it at  $l_i$  for each subscript  $i$ . Here, the sequence  $\{l_0, l_1, \dots\}$  is defined by  $l_i = 50 \times i$ . The data are fitted to the distribution  $D(N, L)$ . We measure the length of the time interval of SAPs from time  $t_1$  at which a knotted SAP appears to time  $t_2$ , at which the next knotted SAP appears after  $t_1$ , and denote it by  $L (= t_2 - t_1)$ .

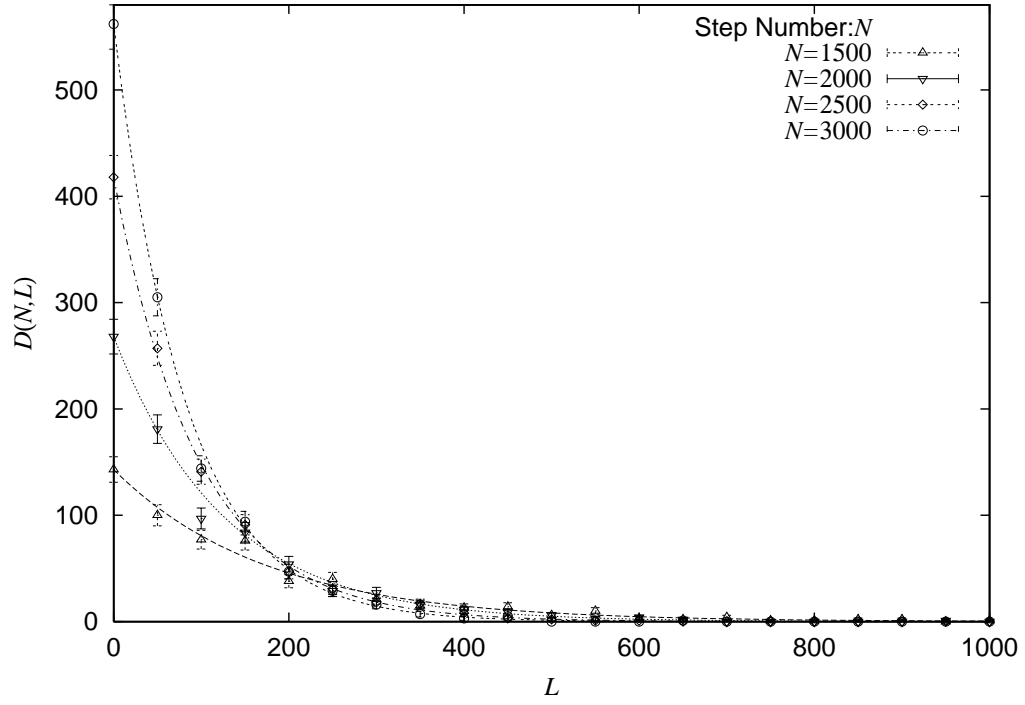


Figure 4b: Discrete Distribution Function of Interval  $L$  of Non-Trivial Knots for  $N = 1500, 2000, 2500$  and  $3000$

We plot the distributions  $D(N, L)$  and the data of  $L$  taking values in  $[l_i, l_{i+1})$  for the step number from  $N = 1,500$  to  $N = 3,000$ , respectively. The data are fitted to  $D(N, L)$  well. Therefore, the MOS pivot generates SAPs without biasing statistics of knots.

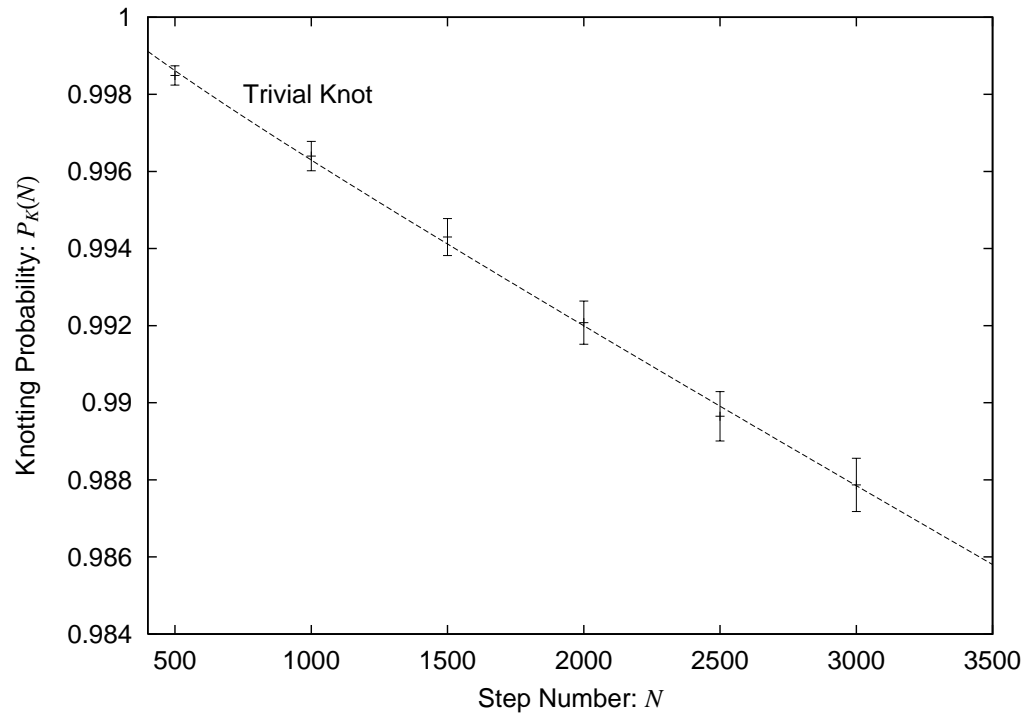


Figure 5: Knotting Probability  $P_\emptyset(N)$

We give the graph of the knotting probability  $P_\emptyset(N)$  for the trivial knot versus the step number  $N$ . Here error bars denote one standard deviation. The data behave the liner decay with respect to  $N$ .

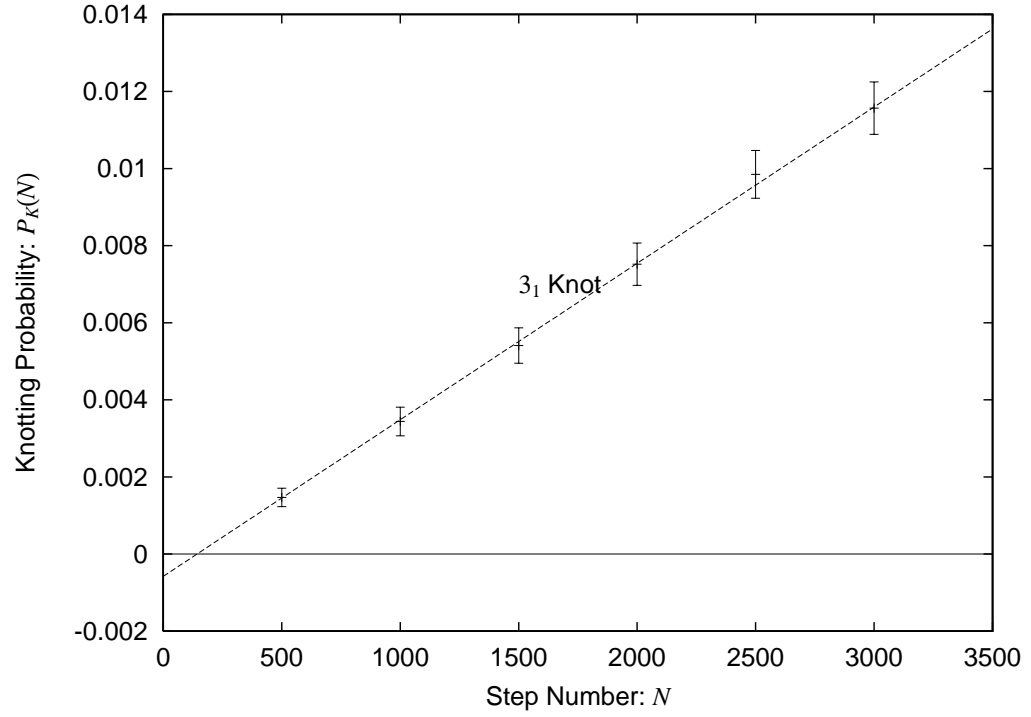


Figure 6: Knotting Probability  $P_{3_1}(N)$

We give the graph of the knotting probability  $P_{3_1}(N)$  of trefoils versus the step number  $N$ . Here error bars denote one standard deviation. If we assume a finite-size effect for the SAPs of trefoils, we fit the data to the straight line which intersect  $x$ -axis at positive value.